JOURNAL OF AIRCRAFT
Vol. 31, No. 1, Jan.–Feb. 1994

Experimental Study of Pneumatic Control of Forebody Vortices at High Alpha

Kenneth C. Cornelius* and Noorulhaq Pandit†
Wright State University, Dayton, Ohio 45435
and
Russel F. Osborn‡ and Robert W. Guyton‡
Wright Laboratory, Wright-Patterson Air Force Base, Ohio 45433

The control of forebody vortex flowfields through the use of pneumatic jets has a significant impact on the maneuverability performance at high angles of attack. Test results of aerodynamic forces on a $\frac{1}{8}$-scale X-29 forebody model were obtained for several nozzle geometries, and the most effective blowing angle was experimentally determined to be 60 deg from the model axis. The most effective nozzle geometry was a converging contraction with an extended, slotted throat region. This nozzle produced a supersonic expansion in two-dimension at a high pressure ratio which resulted in a favorable aerodynamic interaction to enhance the yawing moment at low blowing coefficients. A twofold interaction occurs where the separated vortex flow adjacent to the blowing nozzle moves further around the periphery of the fuselage and the jet/crossflow interaction causes the opposite side vortex to move away from the surface. The asymmetry of the resulting vortex flowfield induces an augmented side force on the fuselage.

Nomenclature

A = forebody reference area, 101.3 cm^2
A_n^* = nondimensional area of nozzle
A_{ref} = wing reference area, 0.269 m^2
C_D = discharge coefficient
C_l = lift coefficient
C_{mz} = $M_m/QA_{\text{ref}}s$, yaw moment coefficient
C_μ = $\dot{m}V_j/QA$, nozzle blowing coefficient
D_n = nozzle throat diameter, 0.059 cm
e = ejector
F = force
k = ratio of specific heats
L = total length of model, 37.8 cm
L_e = length of ejector from nozzle exit
L_s = length of slot for nozzle $S1$
M = Mach number
M_m = moment
$\dot{m}$ = nozzle mass flow rate
n = polytropic coefficient
$(\ )n$ = nozzle
P = static pressure, tunnel
P_r = pressure ratio, P_0/P
P^* = nozzle throat pressure
P_0 = total pressure
Q = dynamic head
R = ideal gas constant
R_l = Reynolds number based on L, 1.2×10^6
s = wing reference span, 103.6 cm
$(\ )s$ = slot
s_e = entropy
w_s = width of slot for nozzle $S1$
$X1, X2$ = nozzle axial location, 6.35, 12.7 cm
(x, y, z) = coordinate axis
α = angle of attack
β = sideslip angle
θ = compressible wave angle
ν = kinematic viscosity
ν_{pe} = Prandtl Meyer expansion angle
ρ = density of air

Introduction

FUTURE air combat will require aircraft maneuver performance that will exceed the capability of present day fighters. At high angles of attack in the poststall region, the aerodynamic control surfaces such as the vertical tail and rudder become engulfed in the separated flowfield of the wing, and lose their ability to impart the yawing moment and side force required for active control of the vehicle. Compounding this problem further, the aircraft is susceptible to asymmetrical side forces generated in the vicinity of the apex of the fuselage or nose region beyond a 30–50-deg angle of attack. These forces arise from the bistable nature of the three-dimensional boundary-layer separation around the periphery of the nose, which leads to unequal strength vortical separations around the forebody. The resulting flowfield may lead to an unstable side force and yawing moment which are detrimental to the controlled motion of the aircraft. This lateral instability must be rectified if poststall multiaxis maneuvering of fighter aircraft is to become a realistic goal.

The key technology that is needed is the extension of aerodynamic control in the poststall regime of the flight envelope. A most promising approach for enhanced dynamic control of the aircraft is the use of properly placed blowing pneumatic jets in the nose region of the forebody, which alters the bistable nature of the asymmetrical development of the vortical separations. This would allow controlled side force and yawing moments to be activated by the variation of the jet momentum. The stability of the vortex flow in the nose region is increased by the use of low aspect ratio strakes on the side of the forebody nose. The vortices generated from the strakes interact with the shed vorticity from the sides of the forebody to provide greater aerodynamic stability throughout an expanded operational flight regime. However, the extension of

Presented as Paper 92-0018 at the AIAA 30th Aerospace Sciences Meeting and Exhibit, Reno, NV, Jan. 6–9, 1992; received June 12, 1992; revision received Oct. 20, 1992; accepted for publication Oct. 24, 1992.

*Assistant Professor, Department of Mechanical and Materials Engineering. Senior Member AIAA.
†Graduate Student.
‡Flight Dynamics Directorate. Member AIAA.

the flight envelope to higher angles of attack, and the increase of the stall/spin resistance, can be limited by the onset of vortex breakdown from either of the individual vortex formations and their interactions with the aircraft control surfaces.

Roll agility in modern fighters is often limited by the onset of lateral-directional instability which can be governed by the bistable vortex separation around the periphery of the aircraft nose. By blowing tangentially to the forebody surface on the leeward side of the vortex in the nose region, various investigators[1-6] have demonstrated significant control and aerodynamic enhancement of maneuverability, where a critical review and bibliography of this technology is available.[7] Both yaw and side force control at high angles of attack can be enhanced by controlling the forebody vortex separation position and strength around the periphery of the nose.

The experimental goal was to determine what configuration, i.e., axisymmetric jet, or variation of jet exit boundary conditions, as well as the angle of the jet relative to the freestream direction would enhance or amplify the favorable jet/vortical interaction with the local aerodynamic forebody surface. Different nozzle geometries were designed and tested on the $\frac{1}{8}$-scale X-29 model forebody. This test explored the impact of altering the forebody vortical separation lines along the fuselage with the desired goal of producing the maximum yawing moment and side force. If the required mass flow rates are in the range of conventional bleed air from the engine, then pneumatics become a viable option for forebody vortex control.

Model Construction

The details of the forebody model configuration used in this study are shown in Fig. 1. The forebody is a replica of the X-29 $\frac{1}{8}$-scale nose forebody. It is constructed from aluminum and has a length of 37.8 cm and a maximum width of 12.3 cm. It was designed in two halves and the internal volume was machined to accommodate an internal balance. Two nozzle blocks were machined separately and mated with the internal surface of the model at two axial positions from the nose apex and symmetrically placed about the centerline. Figure 2 shows a top view of the forebody with nozzle *S1* installed in the first axial location. Figure 3 shows two of the nozzle geometries tested and the nozzle design which allowed individual nozzles to be inserted into the side. O-rings were integrally designed in the nozzle blocks so that each nozzle could be rotated to the desired angle without leakage of the compressed air. The exit plane of the nozzle blocks was configured to be normal to the local surface of curvature of the model at the two axial locations. Nozzle plugs were installed in adjacent ports so that blowing could be exercised from one port at a time.

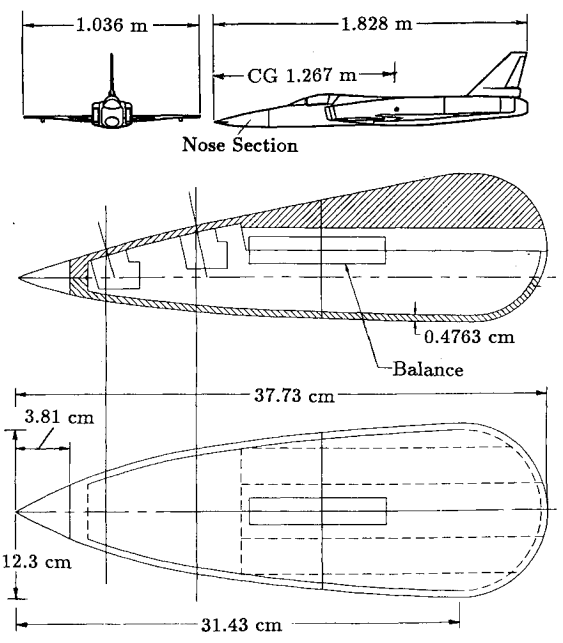

Fig. 1 X-29 Forebody model configuration.

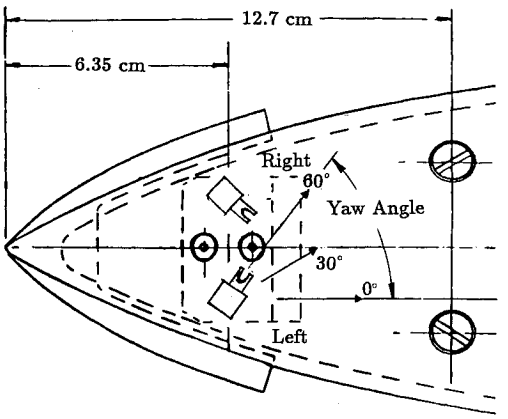

Fig. 2 Top view with nozzle *S1* installed.

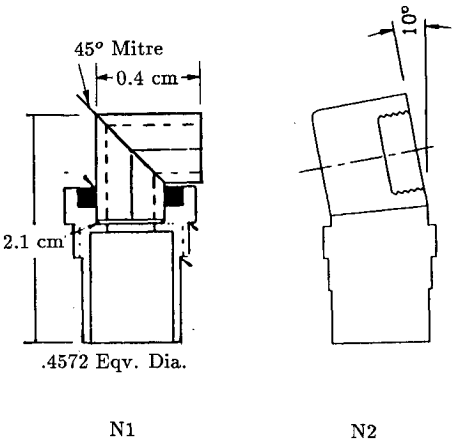

Fig. 3 Nozzle geometries *N1–N2*.

The straked forebody has elliptical cross sections of length 31.43 cm, maximum width 12.3 cm, and height 10.47 cm. The cross-sectional area at the rear of the forebody is 101.3 cm^2 with an equivalent diameter of 11.35 cm which correlates to a nondimensional length $L/D = 2.77$. The rear of the model has a sharp radius with a cutout at the base of the forebody along the centerline to accommodate the model support sting and the flexible air lines. The sting was integrally connected to the internal force balance and the pressure lines were placed symmetrically to the sting to supply compressed air to either side of the nozzle blocks. To insure a fixed separation line at the rear of the forebody, an O-ring was extended above the surface at the beginning of the sharp curvature.

Test Facility

The test was conducted in the Tri-Gas Dynamic Facility Wind Tunnel at the Wright Research and Development Center. The tunnel is fully instrumented and principally dedicated for force measurements about aerodynamic configurations. The TGF tunnel used in this investigation is a closed-return pressure wind tunnel powered by an 8500-hp motor attached to an axial flow compressor. For this study the test section was 0.61 m high, 0.61 m wide, and 6 m in length. The maximum speed utilized in this test was 106 m/s. The freestream speed was controlled by monitoring a set of calibrated Piezzio rings installed upstream of the test section. The model was mounted onto a long sting and cantilevered on the circular turntable to facilitate angle-of-attack changes. The wind tunnel operated with a maximum dynamic head [Q_{max} = 157.4 Nt/m^2 (65 psf)] and $M = 0.3$. The Reynolds number, based

on tunnel freestream velocity and length along the model centerline, was 1.25×10^6. The mass flow was determined by a set of calibrated orifices in series with two pressure lines connected to the nozzle blocks.

Methodology for Development of Nozzles

Many experiments that have been performed in the past, concerning pneumatic vortex flow control, have used 90-deg right-angle nozzles as well as blowing normal to the surface. The right angle nozzles protrude through the surface of the forebody and provide for blowing tangent to the local surface. On investigating the internal flow characteristics of these nozzles, the flow separates around the sharp corner and the separation zone diminishes C_d to a measured value of 0.7. It has been suggested[8] that vortex stability could be influenced by a jet that imparted axial momentum to the outer helical streamlines of the vortex flow. This would favorably amplify the asymmetry of the flowfield about the forebody. Nozzles *N*1–*N*2 in Fig. 3 were designed at the onset of this research to examine this hypothesis. Further experimentation showed that entrainment was curtailed at higher P_r for the right-angle nozzles. To improve the exit flow quality, symmetric contractions from an enlarged cylindrical plenum were designed with an extended throat region. The cylindrical plenum design (*N*2), shown in Fig. 3, allowed individual nozzle geometries to be screwed into the side of the plenum to facilitate easy removal of the individual nozzles. Figure 4 shows one of the nozzles designated as *S*1 that was investigated in the research program.

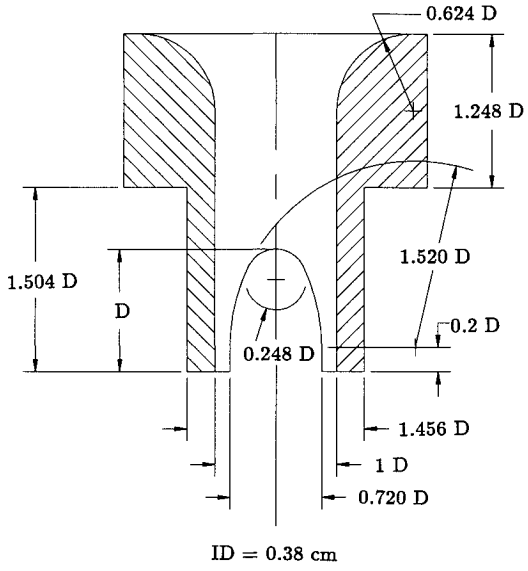

Fig. 4 Sketch of slotted nozzle *S*1.

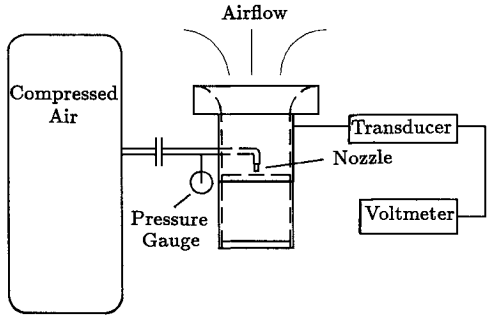

Fig. 5 Experimental ejector arrangement.

It was postulated that greater entrainment in the near field would be advantageous in affecting the greatest asymmetry in the forebody vortex flowfield. A smaller diameter nozzle would also be advantageous from an aerodynamic standpoint which would imply the highest P_r that could be achieved from the engine air bleed, in the range of pressure ratio from 20 to 30. To determine the entrainment rate of each nozzle geometry, a test fixture was designed and built in the form of a conventional ejector with an area ratio of 80 between the primary nozzle and the ejector throat area. The entrainment experiment was designed with the capability to vary the lengths of the ejector body to examine the entrainment rate as a function of the downstream distance. Figure 5 shows a schematic of the experimental setup. This experimental technique was invaluable in optimizing the entrainment for a particular exit geometry at a given P_r. The discharge coefficient as compared to Fliegner's formula[9] for $P_r = 7.8$ was measured as 0.95 for the smooth contoured inlet of each nozzle.

Energy is dissipated across the entropy producing compressive waves for the underexpanded nozzle where the total pressure loss can be significant at the higher Mach numbers. The corresponding entrainment ratio (ejector/nozzle) mass flow rate shown in Fig. 6, with the axisymmetric nozzle placed in the ejector, experiences a significant decay with increasing P_r, indicating that the shock energy losses through viscous dissipation significantly degrades the entrainment capability of this nozzle geometry at higher P_r values. These measurements directed the research effort toward examining asymmetric exit nozzle geometries which would produce weaker oblique shocks downstream with the expressed purpose of eliminating the stronger normal shock dissipation mechanism. Also, if the jet surface area could be increased in the near field, this would provide greater turbulent shear production, thus enhancing the local entrainment. This reasoning led to the optimized nozzle *S*1 shown in Fig. 4. The entrainment ratio at a length of the ejector normalized on the internal diameter of the nozzle of $L_e/D_n = 25$ is shown in Fig. 6. This nozzle has an axisymmetric contraction with an extended throat region. A slot was then milled on ad-

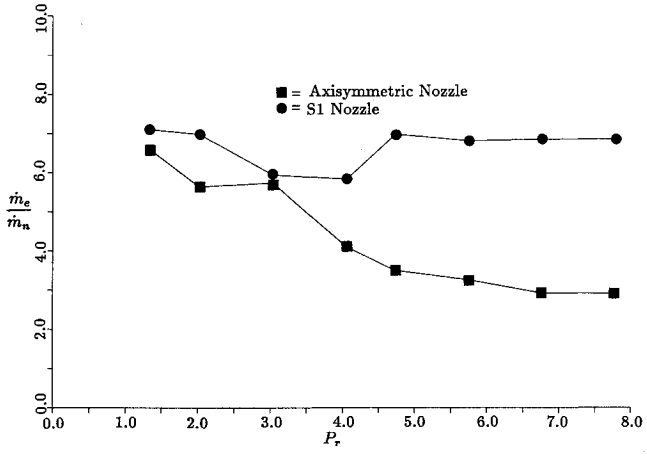

Fig. 6 Entrainment comparison of *A*1 vs *S*1.

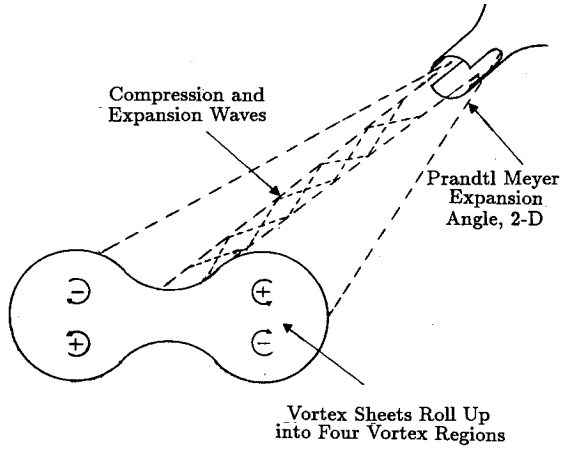

Fig. 7 Physics of supersonic expansion of slotted nozzle.

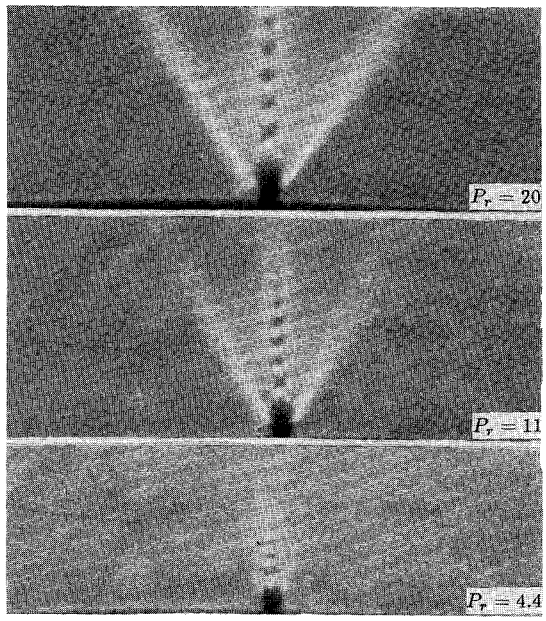

Fig. 8 Schlieren photograph of flow expansion (nozzle *S*1).

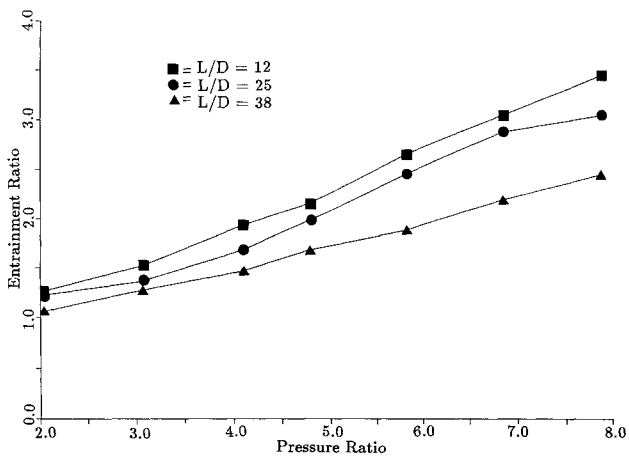

Fig. 9 Entrainment ratio of nozzle (*S*1/*A*1).

jacent sides of the throat region to allow the Prandtl-Meyer expansion of the flow to occur in two dimensions.

A parametric study to maximize the entrainment was obtained for various lengths and widths of the slot. This geometry allowed the jet to expand supersonically into a two-dimensional sheet. The basic physics of the expansion is shown in Fig. 7. Figure 8 shows a schlieren photograph of nozzle *S*1 at $P_r = 20$. The included angle of spread is 82 deg, agreeing with the two-dimensional theory of the Prandtl-Meyer expansion to within 3 deg. The reflected compressive waves reconverge in the center portion of the flow with local oblique expansion and compressive waves. The outer flow escapes the reflected compressive wave reconvergence, since for a fixed Mach number the three-dimensional nature of the expansion must negate the turning of the shear layer. Nozzle *A*1 had an axisymmetric contraction of the same diameter as *S*1 without the extended throat region. The entrainment ratio measurements of nozzle *S*1, normalized on the data for the axisymmetric nozzle *A*1, are shown in Fig. 9 as a function of P_r at various L/D ratios of the ejector. There is greater entrainment by as much as a factor of three at $L_e/D_n = 30$ at the higher P_r.

Theoretical Analysis for Nozzle *S*1

Compressible flow equations[9] along a streamline were used to model the flow for nozzle *S*1. Continuity and conservation

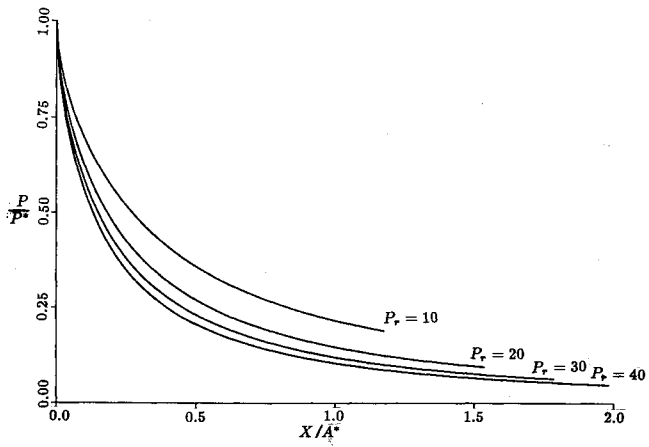

Fig. 10 Pressure distribution through throat region.

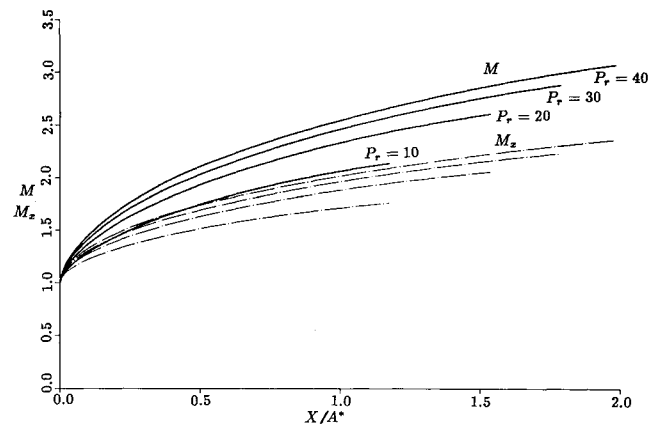

Fig. 11 Mach number variation of nozzle *S*1.

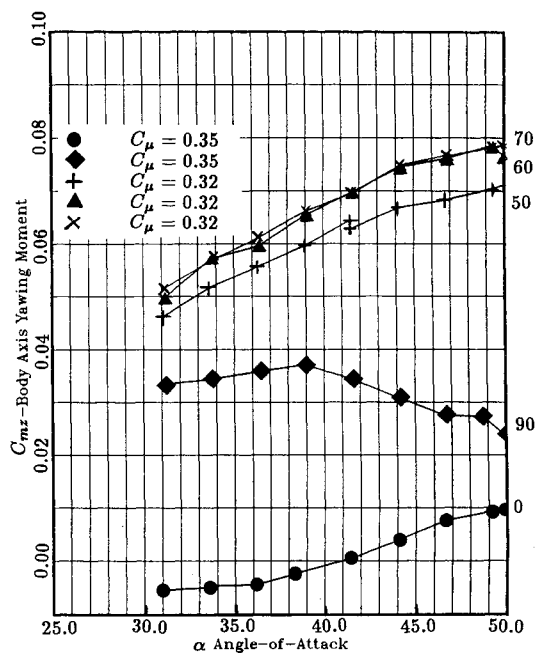

Fig. 12 Angle sensitivity to yawing moment for nozzle *S*1.

of energy and momentum in the x direction were used to develop differential equations for the Mach number along the extended throat region of this nozzle. The polytropic coefficient was found by using the Rankine-Hugoniot relationship for oblique waves which are nonisentropic. $\dot{M}$ represents the derivative with respect to the normalized cross-sectional area

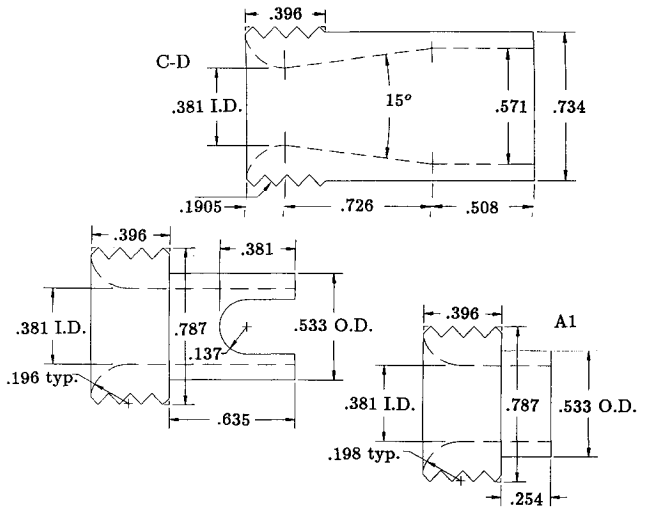

Fig. 13 Exit nozzle geometries *S1*, *C-D*, *A1*.

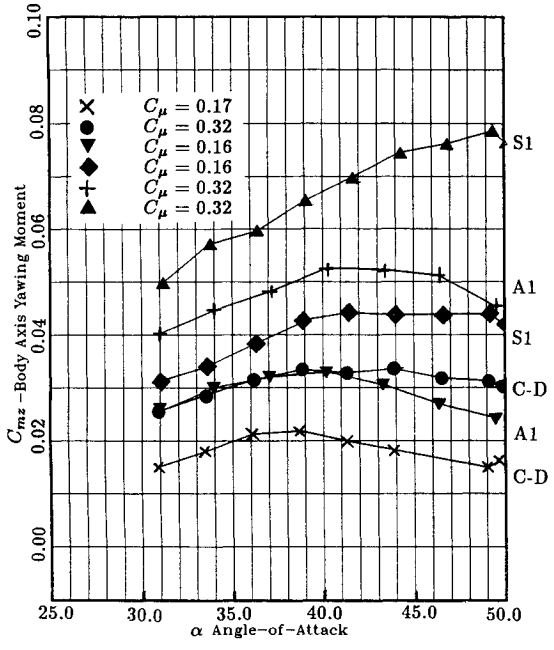

Fig. 14 Yawing moment characteristics for nozzle geometries.

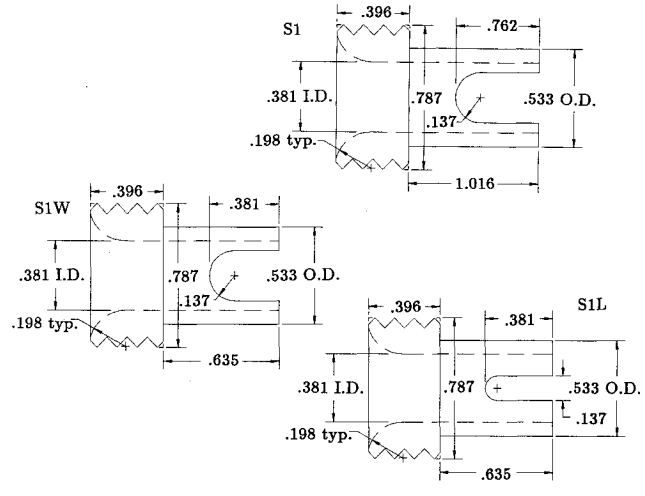

Fig. 15 Sketch of nozzles with varying slot dimensions.

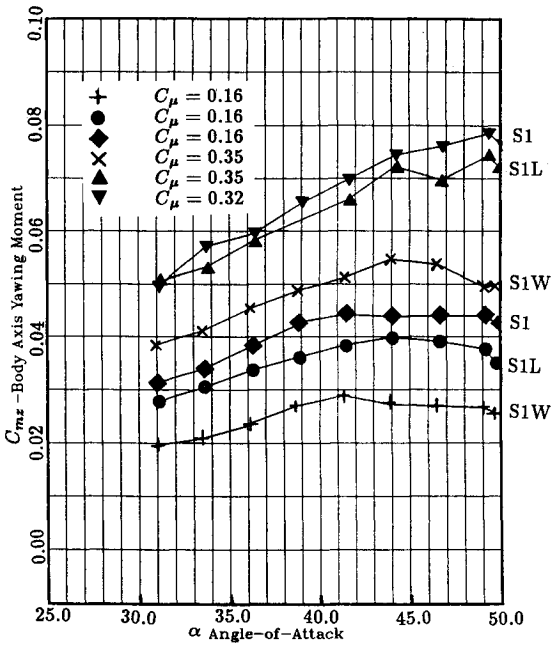

Fig. 16 Yawing moment vs α for various C_μ.

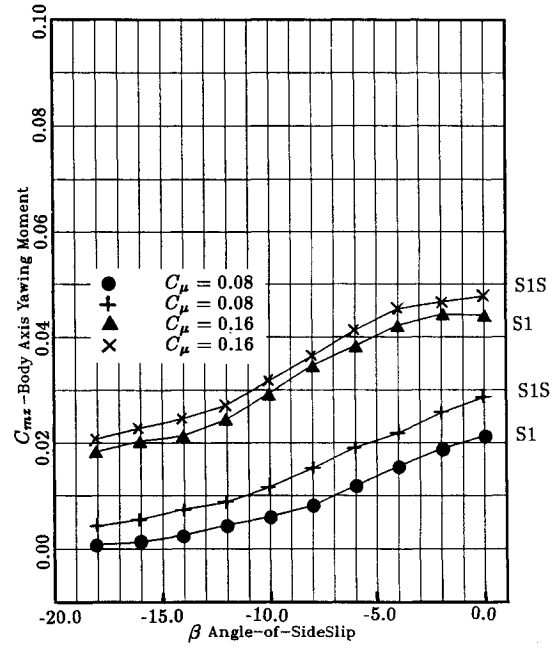

Fig. 17 Yawing moment vs β for $S1S = 0.5\ S1$.

A_n at the throat. The dimensionless equations can be written as

$$\frac{\dot{P}}{P} + \frac{1}{A_n^*} + \dot{M}\left(\frac{1}{M} + \frac{k-1}{1+\frac{k-1}{2}M^2}\frac{M}{2}\right) = 0 \qquad (1)$$

$$M\dot{M}\left(1 - \frac{1}{2}M^2\frac{k-1}{1+\frac{k-1}{2}M^2}\right) + \frac{1}{k}\frac{\dot{P}}{P} + \frac{1}{k}\left(\frac{\dot{s}_c}{R}\right) = 0 \qquad (2)$$

The axial momentum is conserved since the shear stress has been neglected in the analysis. From the Rankine-Hugoniot

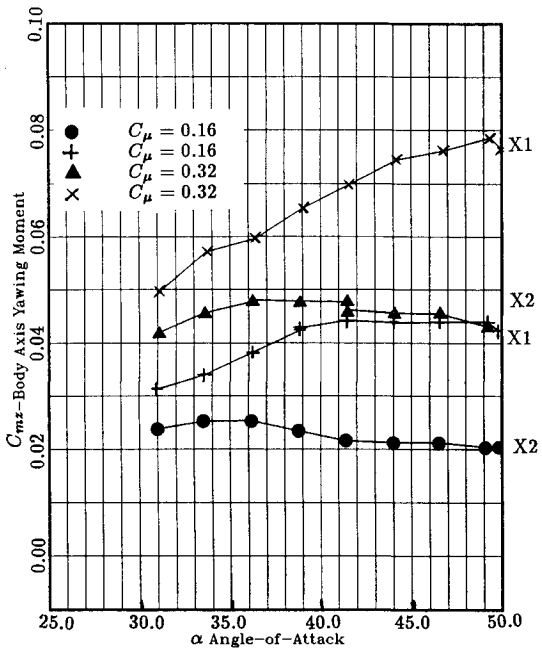

Fig. 18 Yawing moment vs α at two axial locations (*S1*).

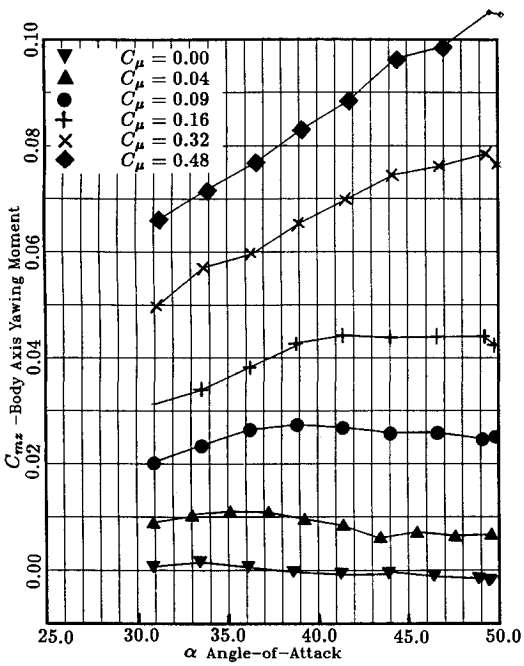

Fig. 20 Yawing moment vs α = (30–50 deg) (*S1*).

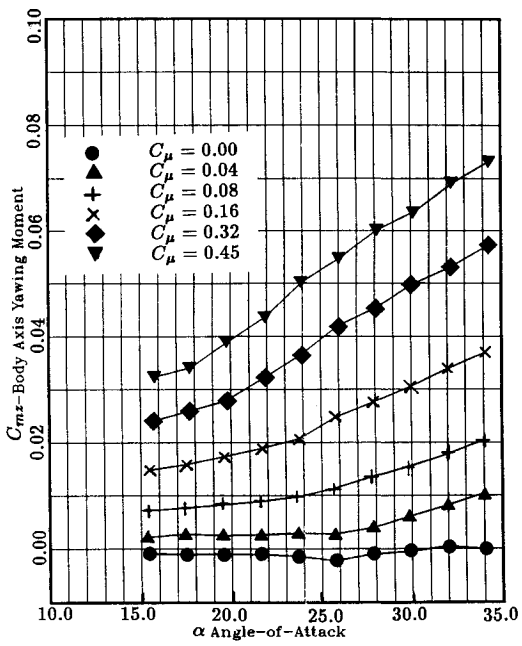

Fig. 19 Yawing moment vs α = (15–35 deg) (*S1*).

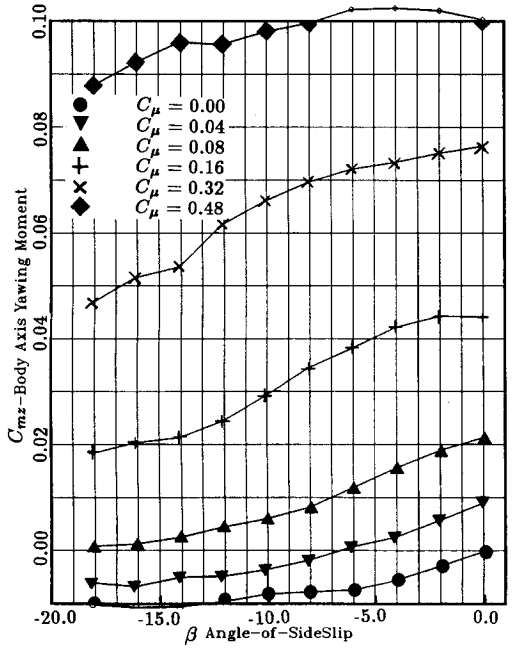

Fig. 21 Yawing moment vs β at α = 45 deg (*S1*).

relation there is a unique relation between P and ρ, defined by the polytropic coefficient where $n > k$:

$$n = k\{1 + [(k - 1)/k](M_x^2 \sin^2\theta - 1)\} \tag{3}$$

The entropy equation can be expressed as

$$\frac{\dot{s}_e}{R} = \frac{2k}{k+1}(M_x^2 \sin^2\theta - 1)\left[\left(\frac{n-1}{n}\right)\left(\frac{k}{k-1}\right) - 1\right] \tag{4}$$

The curves of the dimensionless pressure vs the dimensionless length are shown in Fig. 10 for different supply pressure ratios. It can be inferred from the graph that beyond a dimensionless length of one there is not a significant difference between the integrated area under the curves. Therefore, a nozzle *S1* with $L_s/D_n = 1$ was chosen for the forebody blowing test. The curves of Mach numbers along the extended region of the slot including the spatial average of M_x and the corresponding Mach number along the streamline M are also plotted against the dimensionless length in Fig. 11. The compressible flow is predominantly isentropic throughout the expansion of the throat region.

Aerodynamic Force Data

The $\frac{1}{8}$-scale forebody was designed to accommodate a six-component internal force balance. The flexible pressure lines for the compressed air bridged the model and sting to provide for metric data. Pressure tares were measured and subtracted from the balance measurements. The yawing moment C_{mz} for the vertical stabilizer has a magnitude 0.06 with rudder fully deflected on the full $\frac{1}{8}$-scale model as reported.[4] Beyond a 20-deg angle of attack, the rudder begins to lose effectiveness in providing a restoring yawing moment to the aircraft, and at

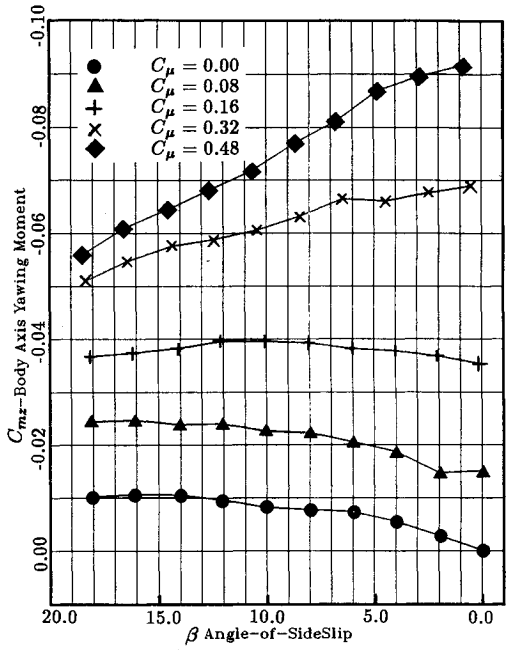

Fig. 22 Yawing moment vs β at α = 45 deg (*S1*).

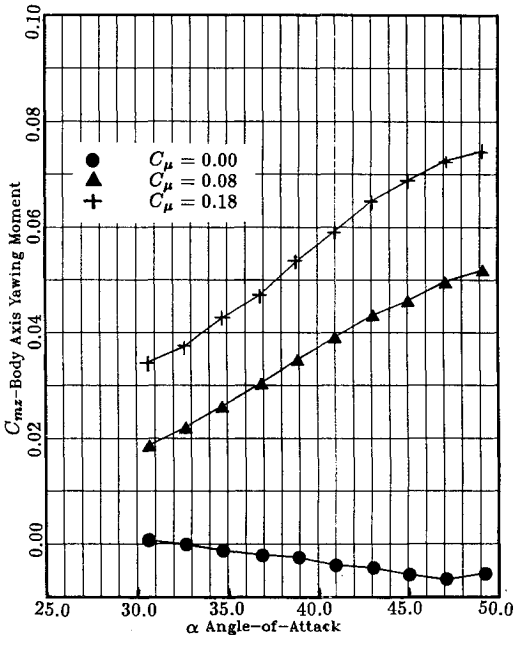

Fig. 23 Yawing moment with noseboom, no strakes (*S1*).

48 deg there is no rudder control. These two characteristics limit the flight envelope of the aircraft and decrease the high-angle-of-attack maneuverability and agility of the vehicle. Only the data from blowing on the right side of the nozzle is presented below, since blowing on the left side was symmetrical (with forces and moments in the opposite direction) with the right side to within 6%. The blowing coefficient C_μ was normalized on the afterbody cross-sectional area.

Yawing Sensitivity of Nozzles

The nozzle *S1* was pointed at different angles relative to the axis of the model and Fig. 12 shows that the maximum gain on the yawing moment occurs at a pointing vector of 60 deg from the axis of the model. Figure 2 shows a sketch of the nozzle orientation for nozzle *S1* canted inboard at 60 deg with the slot vertical. The corresponding data for nozzle *N1* showed similar trends with the nozzle orientation, but with a reduction of 30% in magnitude in C_{mz}.

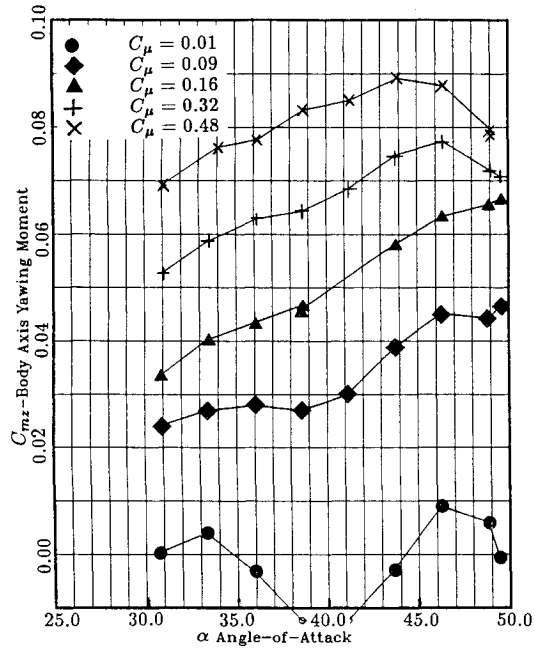

Fig. 24 Yawing moment with no strakes (*S1*).

Comparison of Exit Nozzle Geometries

Figure 13 shows a sketch of the various exit geometries which could be individually inserted into the nozzle plenum. Different nozzle exit geometries were investigated with the pointing vector at 60 deg from the model axis. Figure 14 shows the comparison of an axisymmetric (*A1*), converging-diverging (*C-D*), and slotted nozzle (*S1*). The greatest amplification of the yawing moment was nozzle *S1* with the slot positioned in the vertical plane.

Sensitivity of Nozzle *S1* with Slot Dimension

Three slot dimensions, shown in Fig. 15, were investigated to examine the sensitivity of this parameter on the yawing moment. Figure 16 shows that nozzle *S1* with slot dimensions L_s/D_n = 1 and w_s/D_n = 0.72 is the optimum configuration. A smaller throat diameter nozzle *S1S* = 0.58 *S1* was fabricated to examine the sensitivity to P_r. Figure 17 shows a 20% improvement in yawing moment for an equivalent C_μ. These data emphasize that higher P_r allows the scaling to a smaller physical dimension for equivalent C_μ.

Nozzle Axial Position

The nozzle blocks accommodated two axial positions *X1* and *X2* in which the nozzles could be inserted. Figure 18 shows that by positioning the nozzles closer to the apex of the nose, greater magnitude of the yawing moment can be achieved.

Effect of *Cu* for the Angle-of-Attack Range

Figures 19 and 20 show the model C_{mz} vs angle of attack at various blowing coefficients throughout the angle-of-attack range. At the 15–35-deg range shown in Fig. 19 the positive gradient of yawing moment commences at lower angles of attack as the blowing coefficient increases. Figure 20 demonstrates that the effect of the jet/vortex interactions levels off at the lower blowing coefficients.

Yawing Moment with Sideslip Angle

Figure 21 shows the yawing moment variation with nozzle *S1* blowing on the right side at the optimized angle with sideslip angles from 0 to −20 deg, and Fig. 22 shows the corresponding sideslip angles from 0 to 20 deg with the model at an angle of attack of 45 deg. The curves demonstrate that an increment in C_{mz} can be activated at large sideslip angles.

Yawing Moment Without Forebody Strakes

Figure 23 shows yawing moment data with the strakes removed from the forebody. The yawing moment is significantly greater at lower C_μ, with the jet yawed 60 deg from the freestream direction. This data is consistent with earlier observations of different aspect ratio strake configurations reported,[10] i.e., with no strakes the yawing moment produced by blowing has more amplification at the lower blowing rates. Figure 24 shows the yawing moment without the strakes on the forebody, with a noseboom extended in front of the forebody with the same jet orientation. With no blowing, the yawing moment meanders to either side of the equilibrium position as the angle of attack is varied. With no strakes, the yawing moment produced by blowing has more amplification at the lower blowing rates.

Conclusions

A parametric study incorporated various nozzle geometries in the forebody with variable blowing rates, to study the effect of enhanced entrainment rates on the dynamics of the jet/vortex flowfield. The data from a six-component balance provided insight into the integrated effect of the interactions on the aircraft forebody surface. A nozzle geometry, designated *S1*, has a symmetric contraction with an extended slotted throat region which shows greater entrainment magnitude as compared to axisymmetric nozzles at higher P_r. This configuration allows the jet to expand supersonically into a two-dimensional sheet which provides for greater aerodynamic interaction between the expanding jet flow and the flowfield about the forebody. Significant amplification of the yawing moment, when the jet is yawed 60 deg from the downstream model axis in comparison to blowing along the axis, has been demonstrated.

The ramifications of altering the vortex flow pattern are apparent from these results. A pneumatic jet placed in the nose region and canted inboard 60 deg from the body axis has the following favorable characteristics in terms of amplifying the side force for a fixed blowing coefficient:

1) A nozzle which undergoes a supersonic expansion in the vertical plane and is yawed 60 deg to the forebody axis shows the greatest sensitivity in augmenting the yawing moment for a fixed blowing coefficient.

2) By blowing across the forebody the vortex flow adjacent to the blowing jet becomes stabilized, moving the separation line further around the fuselage. The jet/crossflow interaction across the centerline of the model pushes the adjacent vortical core away from the surface, producing a twofold effect on the asymmetry.

Acknowledgments

This research was performed at the Flight Dynamics Laboratory, Wright-Patterson Air Force Base under Contract F49620-88-C-0053/SB5881-0378 from Office of Scientific Research (AFOSR). The authors would like to acknowledge the helpful discussions with John Tinnapple from the Instrumentation Group for his support throughout this project.

References

[1]Skow, A. M., Titiriga, A., and Moore, W. A., "Forebody/Wing Vortex Interactions and Their Influence on Departure and Spin Resistance," High Angle of Attack Aerodynamics, AGARD CP-247, Oct. 1978.

[2]Skow, A. M., and Peake, D. J., "Control of the Forebody Vortex Orientation by Asymmetric Air Injection," AGARD CP-262-15, May 1979.

[3]Peake, D. J., Owen, F. K., and Johnson, D. A., "Control of Forebody Vortex Orientation to Alleviate Side Forces," AIAA Paper 80-0183, Jan. 1980.

[4]Guyton, R. W., Osborn, R. F., and LeMay, S. P., "Forebody Vortex Control Aeromechanics," AGARD Fluid Dynamics Panel, Paper 16, Toulouse, France, May 1991.

[5]Guyton, R. W., and Maerki, G., "X-29 Forebody Jet Blowing," AIAA Paper 92-0017, Jan. 1992.

[6]LeMay, S. P., Sewall, W. G., and Henderson, J. F., "Forebody Vortex Flow Control on the F-16C Using Tangential Slot and Jet Nozzle Blowing," AIAA Paper 92-0019, Jan. 1992.

[7]Ericsson, L. E., "Control of Forebody Flow Asymmetry, A Critical Review," AIAA Paper 90-2833, Sept. 1990.

[8]Cornelius, K. C., "3-D Analysis of Laser Measurements of Vortex Bursting on a Chined Forebody Fighter Configuration," AIAA Paper 90-3020, Aug. 1990.

[9]Shapiro, A. H., *The Dynamics and Thermodynamics of Compressible Fluid Flow*, Vol. 1, Ronald Press Co., 1953.

[10]Malcomb, G. N., Ng, T. T., Lewis, L. C., and Murri, D. G., "Development of Non-Conventional Control Methods for High Angle of Attack Flight Using Vortex Manipulation," AIAA Paper 89-2192, Sept. 1989.